RSC Advances

ROYAL SOCIETY OF CHEMISTRY

www.rsc.org/advances

Journal Name

Research Article

Acid functionalized MWCNT/PVP nanocomposite as new additive for fabrication of ultrafiltration membrane with improved anti-fouling resistance.

Masooma[a,b], Hatijah Basri[a], M.Irfan[c], Woei-Jye Lau[b].

Received 00th January 20xx,
Accepted 00th January 20xx

DOI: 10.1039/x0xx00000x

www.rsc.org/

Abstract:

Membrane fouling is one of the main challenges encountered in ultrafiltration (UF) processes and the use of nanoparticles for the improvement of UF performance is a recent trend in membrane technology. In this study, in order to improve surface characteristics of polyethersulfone (PES)-based membrane for greater resistance against biofouling, the PES was incorporated with a new type of nanocomposite (NC) in which the NC could be synthesized by blending acid functionalized multiwalled carbon nanotube (f-MWCNT) with Polyvinylpyrrolidone (PVP) in dimethylformamide (DMF). The chemistry of the NCs embedded within the PES membrane matrix was analysed by FTIR, whereas the fabricated membranes were characterized by FESEM, contact angle, water absorption tests, surface profile studies and their filtration performances with respect to pure water permeation, antifouling resistance against protein and flux recovery rate. Results revealed that, compared to the pristine PES membrane, the antifouling ability of PES membrane incorporated with f-MWCNT/PVP NC is greater, recording 81.7% flux recovery and 80.2% total resistance (>76% were reversible one). The protein separation results indicated that, the NCs based membrane was able to reject 93.4%, 74.7%, 59.4% and 28.5% for bovine serum albumin (66 kDa), pepsin (34.6 kDa), trypsin (20 kDa) and (14.6 kDa), respectively.

1. Introduction:

Methods for protein concentration and separation are in high demand due to the rigorous requirements for high-purity protein [1-3]. Several separation methods such as ultrafiltration (UF) [4, 5], tangential flow filtration[6], adsorption[7], and electrophoresis membrane contactors [8] have been applied in the concentration and separation of proteins from their mixtures. Among these methods, UF has been extensively adopted in the isolation and purification of proteins because it does not require large quantities of salts and buffers, offers continuous operation and eliminates some of the troublesome aspects related to chromatography techniques [3, 4, 8].

Polymeric UF membranes are the key component for more efficient use of UF processes in purification and separation of proteins. Most of the commercial UF membranes are fabricated from hydrophobic/semi-hydrophobic polymers such as PES, Polysulfone (PS), polypropylene (PP) and polyvinylidene fluoride (PVDF), by the phase inversion method [9]. Among which PES is one of the most broadly used polymers for UF membrane making.

Polyethersulfone is a thermoplastic polymer having excellent chemical and thermal stability as well as high mechanical strength [10]. Despite the advantages as a membrane material, PES itself is not hydrophilic enough and thus the water permeability of PES membrane is not satisfactory in practical applications. It is also susceptible to serious membrane fouling, leading to the gradual decrease of permeation flux and frequent membrane washing [11, 12]. Therefore, PES-based membrane is often modified to improve its hydrophilicity, anti-fouling ability and filtration properties before its practical use.

In recent years, inorganic materials have received more and more attention in membrane modification. By introducing inorganic materials into the organic membrane matrix, organic–inorganic hybrid membranes that combine the basic properties of organic and inorganic materials could be demonstrated. These include enhanced separation performance, promising anti-fouling ability, good thermal and chemical stability as well as greater adaptability to harsh environments [13, 14]. Zirconium oxide (ZrO_2), titanium oxide (TiO_2), zeolite, mesoporous silica (SiO_2) and carbon nanotubes (CNTs) are some of the examples of inorganic fillers that have been previously used to fabricate hybrid UF membranes with improved antifouling capacity [15-18]. Among these materials, CNTs have gained significant attention whether in laboratories or industries, owing to their rapid mass transport behavior caused by large surface area, in combination with excellent mechanical, electrical and thermal properties.

Nevertheless, direct use of CNTs without surface modification for membrane making is likely to cause a poor distribution of

[a] *Department of Science, Faculty of Science, Technology and Human Development, Universiti Tun Hussein Onn Malaysia, Parit Raja, Batu Pahat 86400, Johor, Malaysia.*
[b] *Advanced Membrane Technology Research Centre (AMTEC), Universiti Teknologi Malaysia, 81310 UTM, Skudai Johor, Malaysia.*
[c] *Department of Bioprocess Engineering, Faculty of Chemical Engineering, c/o Institute of Bioproduct Development, Universiti Teknologi Malaysia, 81310 UTM Johor Bahru, Johor, Malaysia.*
** **Corresponding author**. Hatijah Basri[a] ,Tel : +6074537987; Fax : +6074536051. Email address: hatijah@uthm.edu.my*

nanofillers in the membrane matrix, creating defects on membrane surface. These negative features are mainly attributed to the agglomeration of CNTs in the polymeric dope solution [19-23]. Salvetat et al. further reported that poor dispersion of CNTs could lead to drastic weakening of the polymer composites and affected the mechanical and functional properties of CNTs/polymer composites [24-26].

To enhance the properties of CNTs as active reinforcements, mechanical approach (e.g. ultrasonication/high stirring mixing [27-29]) and chemical modification (e.g. acid functionalization[30, 31]) are generally considered.. The chemical-based approach however is still the most effective way to achieve the desired properties. Upon acid functionalization, the modified multiwalled carbon nanotubes (MWCNTs) were reported to disperse better in the polymer matrix [32]. It is because the introduction of carboxylic acid (–COOH) and hydroxyl (–OH) groups on the surface of MWCNTs tended to enhance the ionic character of the nanotubes, resulting in improved dispersion in polar solvent. On the other hand, in order to improve the hydrophilicity of PES, PVP is commonly used as the hydrophilizing additives. It inhibits the protein adsorption on the membrane surface and increases the flux recovery ratio with reversible protein resistance. PVP is also highly polar, non-ionic, physiologically inert, amphiphilic and water-soluble polymer, it can swell in aqueous media and alter the membrane characters during actual performance [33-35]. It has been previously reported that PVP could play an important role to reduce the aggregation effect of MWCNTs and further improve its disperse ability in different solvents [36]. However, it must be pointed out that the nanocomposites of PVP with functionalized MWCNTs (f-MWCNTs) are rarely been reported in the study of protein separation and antifouling of UF membrane. Surface modification of MWCNTs is required in order to enhance their bonding behavior toward hydrophilic molecules via hydrogen bonding [37, 38]. **Fig. 1.** illustrates the interaction of PES membrane with MWCNT/PVP NC via hydrophobic-hydrophobic interaction or π-π stacking**.**

Figure 1

Chang et al. [39] fabricated the graphene oxide/PVP based PVDF membrane via hydrogen bonding and Van der Waals force. It is observed that without graphene oxide, the increasing amount of PVP tended to create larger pores in PVDF/PVP membranes. Besides, most of the PVP was washed away during the phase inversion process. According to the authors, the use of graphene oxide was likely to interact with PVP via its hydroxyl/carboxyl functional groups, reducing PVP leaching and enhancing the anti-fouling properties of membranes. Wang et al. [40] on the other hand, coated mussel-inspired dopamine on the surface of commercially available UF and microfiltration (MF) membranes through one-step polymerization. Results showed that in addition to the greater water flux achieved, the surface-modified membranes demonstrated superior antifouling properties during protein-rich water and oil-in-water emulsion treatment processes. These studies suggested that appropriate modification of the membrane surface could improve the antifouling performance of the pristine polymeric membranes.

The objective of this work is to expand the scope of using f-MWCNT/PVP based NCs to produce potentially high performance antifouling UF membranes that made of PES polymer. MWCNTs were acid-functionalized in order to improve their dispersion and develop hydrogen bonding with PVP and PES. The influence of novel NCs on the PES membrane properties was further studied based on FESEM, contact angle and water absorption measurements. The membrane surface profile was extensively described in terms of diameter, area, volume, length, and perimeter of surface grain by AFM. The protein adsorption results with flux recovery, the total resistance rate, the reversible resistance and the irreversible resistance studies were discussed in detail with the membranes antifouling performances.

2. Materials and methods

2.1 Materials

PES, (Ultrason E6020P) having an average molecular weight (MW) of 58,000 g/mol was purchased from BASF, Germany. DMF [(HCON $(CH_3)_2$; MW = 80.14 g/mol] of 99.8% purity was purchased from Labscan Asia Co., Ltd. Pristine MWCNTs (color: black, purity: >98%, length: 12 µm, avg. diameter: 10 nm and true density : 0.05 g/cm^3) were purchased from Chengdong (China). Bovine serum albumin (BSA, 66 kDa), pepsin (35 KDa), trypsin (20 KDa) and lysozyme (14.6 kDa) were purchased from Sigma-Aldrich. Other chemicals used in this work were of analytical grade and used without purification.

2.2 Acid functionalization of MWCNTs

The purpose of acid functionalization of raw MWCNTs is not only to remove impurities of metallic catalysts from CNTs but also to introduce polar carboxylic (-COOH) and hydroxyl (-OH) functional groups. 4 g of MWCNTs was treated with a mixture of nitric and sulfuric acid in the ratio of 3:1 in a flask equipped with a condenser and a stirrer at the 110 °C for 24 h. The solution was diluted with 1 L of de-ionized (DI) water and filtered through a 0.22 µm polycarbonate membrane. The synthesized f-MWCNTs were washed with DI water until the pH of the filtrate became 7. It was followed by drying in an oven [38, 41].

2.3 Membrane fabrication

The dope solutions of different membranes were prepared according to the formulation shown in **Table 1.** At first, different NCs were synthesized by blending PVP and f-MWCNTs for 6 h in DMF until the homogeneous dispersion was obtained. It was followed by the addition of PES at 80°C. The solution was continuously stirred overnight in order to completely dissolve the PES. Upon completion of stirring, the dope solution (PES/f-MWCNT/PVP nano-hybrid solution) was cooled down naturally to room temperature before pouring into the storage bottle. The ultrasonic bath was used to remove the air bubbles from the dope solution. The viscosities of dope solutions were then measured using digital rheometer (DV-III, Brookfield) equipped with a sample

adaptor (SC4-31) at 25°C [42]. Flat sheet membranes were made using non-solvent induced phase inversion process. At first, the polymer solution was spread on a dust free glass plate. The dope was cast using a casting knife with a thickness of 200 μm followed by immediately placed in a coagulation bath of DI water at room temperature. After the post treatment with hot water at 90°C for 30 min, the resultant membranes were stored in water container until use. Post treatment is necessary to remove loosely blended NCs from PES matrix and minimize membrane shrinking.

Table 1:

2.4 Characterization

2.4.1 f-MWCNT, f-MWCNT/PVP and membranes

The surface functional groups of the f-MWCNTs were determined using FTIR (Spectrum One B, Perkin-Elmer). Prior to analysis, all the f-MWCNTs were heated to 70°C for 2 h to remove water content. Same approach was used to analyse the chemistry of the NCs and membrane samples prepared in section 2.3. The scanning range of the experiment was 375–4000 cm^{-1} and during the analysis, the number of scans with the air as the background was kept constant. The XRD patterns of the MWCNTs with and without acid functionalization were measured at 2θ ranging from 10^{o} to 80^{o} (0.1° step size and 1 second/step) using XRD instrument (D8 Advance X-ray, Bruker).

2.4.2 Membrane morphology

The cross section morphology and surface topography of membranes were determined using FESEM (JEOL JSM-7500F). The membrane sample was snapped in liquid nitrogen and followed by sputter-coated with platinum and mounted onto brass plates using double-sided cellophane tapes in a lateral and frontal positions.

2.4.3 Contact angle and water absorption

An optical contact angle measurement system using dynamic, sessile drop method (CAM 101 optical Contact Angle Meter, KSV Instruments) and water absorption was used to determine the surface hydrophilicity of the fabricated membranes. For the water adsorption experiment, the membrane samples (5 cm × 5 cm) were dried in an oven at 60°C for 2 h before testing and then weighed (M_{dry}). The pre-weighted sample was soaked in DI water at room temperature for the next 48 h. Wetted membrane (M_{wet}) was then weighed again after removing water from the surface with tissue paper. The water uptake of the membrane (%) was determined using **Eq. 1** [43, 44].

$$Water\ uptake = \frac{M_{wet} - M_{dry}}{M_{dry}} \times 100 \qquad (1)$$

2.4.4 Surface roughness by line statistics table and 3D pictures

The 3D micrographs with quantitative measurements of line statistics quantities were analyzed using the AFM (Park XE-100). For the scanning, contact mode was used and all roughness parameters of membranes were determined by an XEI-AFM standard software program from the AFM scanned images (2.5 μm × 2.5 μm). In the line statistics table, Min, Max, Mid and Rpv symbolize the minimum height, maximum height, the average between the minimum and maximum height and peak-to-valley respectively, whereas Rq, Ra, Rz, Rsk and Rku correspond to root-mean-squared roughness, roughness average, ten points average roughness, skewness and kurtosis of the line, respectively.

2.4.5 Surface profiles via grain analysis

XEI-AFM standard image processing and analysis software was used for the detection of different grains on the membrane surface. In the grain analysis, the software automatically detects the grains in the loaded image, calculates the length, volume, area and perimeter of each detected grain and then pore radius and diameters were mathematically calculated by using the obtained data (length and volume). The watershed method was used for detection of grain on the surface of membranes. According to that, if water is poured over the membrane surface, then water after filling one grain will start to overflow to other neighboring grains and thus more grains are detected. Algorithm recognizes this point and sets the grain boundaries in terms of surface profiles [45].

2.4.6 Water flux and fouling test

Cross flow cell having an effective area of $42cm^2$ was used to calculate the pure water permeation (J_{w1}, J_{w2} and J_{w3}) and protein flux (J_p) through differently formulated membranes. DI water was utilized for the experiments at the pressure of 2.75-3.0 bars at room temperature. Membrane pure water flux (J_{w1}) was calculated using **Eq. (2).**

$$j_{w1} = \frac{V}{t \times A} \qquad (2)$$

where V (L) is the volume of permeate, A (m^2) is the effective area of the flat sheet membrane and t (h) is the UF time. UF experiment was continued to determine the antifouling property of membranes; UF experiment was continued by replacing pure water with feed protein solution containing 1000 ppm BSA. The experiment was performed under the same condition for the next 1.5h and BSA flux was noted as 'J_p'. After that, the feed solution tank was refilled with DI water and the membrane was cleaned by allowing the DI water to flow for 30 min under the same condition as a pure water permeability test. Then, pure water flux (J_{w2}) was re-measured. The experiment was continued in the 2nd round and again DI water was replaced by the BSA solution followed by washing and measurement of flux as J_{w3} to obtain the flux recovery percentage (R_{FR}) as expressed in **Eq. (3)**[46]**.**

$$R_{FR}(\%) = \frac{J_{w3}}{j_{w1}} \times 100 \qquad (3)$$

Generally, the fouling of UF membrane is caused by reversible and irreversible ones. Reversible fouling can be simply removed by washing with water. However, irreversible fouling remains after washing unless more drastic chemical cleaning is applied. To better

analyze the mechanism, the total resistance rate (R_t), the reversible resistance (R_r) and the irreversible resistance (R_{ir}) rate were calculated using **Eqs. 4, 5 and 6** respectively [47, 48].

$$R_t(\%) = (1 - \frac{J_{p3}}{J_{w1}}) \times 100 = R_r + R_{ir} \quad (4)$$

$$R_r(\%) = \frac{J_{w3} - J_{p3}}{J_{w1}} \times 100 \quad (5)$$

$$R_{ir}(\%) = \frac{J_{w1} - J_{w3}}{J_{w1}} \times 100 \quad (6)$$

2.4.7 Protein adsorption studies

To determine the adsorbed amount of BSA, static and dynamic protein adsorption experiments were performed on the prepared membranes at pH ≅7. Small pieces of membranes were immersed into vials containing 10ml of BSA solution (1 g/L) in 10 mmol/L phosphate buffer of pH ≅ 7. The HCl and NaOH aqueous solutions (0.1 M) were used to maintain the pH. In the static method, the vials were placed on the stable horizontal table, whereas in the dynamic method, the vials were kept on the water shaker for 6 h at room temperature (25°C). Afterward, the membranes were removed from protein solutions and the concentration of BSA in the supernatant solutions was determined using Bradford reagent. The adsorbed amounts of BSA on the membranes were determined from the change in concentration of the BSA solution before and after the adsorption via calibration curve method [46].

2.4.8 Protein rejection

Protein transmission experiments were conducted at pH ≅ 7 and 0.05 N HCl and NaOH solution were used to maintain the pH. Four types of proteins (66-kDa BSA, 34.6-kDa pepsin, 20-kDa trypsin and 14.6-kDa lysozyme) were used. The feed container was filled up with 250 mL solution of proteins (1000 ppm) and UF was performed for 30 min at 2.75-3.0 bar. The protein rejection R (%) was calculated using **Eq. 7**.

$$R = (1 - \frac{C_p}{C_f}) \times 100 \quad (7)$$

where C_p and C_f are the protein concentrations (ppm) in permeate and feed solution, respectively. Micro BCA™ protein assay reagent kit was used to determine the amount of protein through calibration curve method.

3.0 Results and discussion

3.1 f-MWCNTs /PVP based NCs

DMF was used as the solvent for f-MWCNT, NCs and membrane formation and the solvent solubility parameter was used for the selection of proper dispersion of f-MWCNT in DMF [49]. Acid functionalization of MWCNTs produces polar (carboxyl and hydroxyl) functional sites on the surface of MWCNTs which contributes not only to its homogeneous distribution in DMF but also the creation of hydrogen bonds with nitrogen and hydrogen atoms that, present in the PVP molecules (see **Fig. 1.**) [50, 51] **Fig. 2** shows the FTIR spectra of the MWCNT, f-MWCNTs, pure PVP and different NCs. The differences between FTIR spectra of raw and modified MWCNTs show that new peaks detected at 2950 cm^{-1} and 3450 cm^{-1} in the f-MWCNT corresponded to the O-H of acid and alcohol. Peak existed at 1030 cm^{-1} on the other hand could be attributed to primary alcohol R—O—H (1025-1060 cm^{-1}) [52]. These peaks confirmed the attachment of acid and alcohol functional groups onto the f-MWCNT surface. With respect to the spectra of PVP, the band found at 1698 cm^{-1} was related to the pyrrolidone C=O group while the bands at 1031 cm^{-1}, 1260 cm^{-1} and 1427 cm^{-1} were due to C-C stretching vibration, C-N stretching vibration and C-H bending vibration of PVP, respectively [53].

In the FTIR spectra of different f-MWCNT-PVP NCs produced (see **Table 1**), three sharp peaks were observed in each NC at 1650, 2900 and 3400 cm^{-1}. These peaks belong to a tertiary amide, alcohol and –OH of acids, respectively. To confirm the existence of hydrogen bonding, one can observe that peaks became broadened or sharpened and moved to lower absorption frequency [54]. Compared to the FTIR spectra of f-MWMCT and PVP, the peak at 3400 cm^{-1} was changed and became broadened. Also, the presence of a sharp peak at 1640 cm^{-1} confirmed the presence of hydrogen bonding in all NCs.

Figure 2:

The chemical functionalization of MWCNTs is also confirmed by the XRD results (see Fig. 3). The obtained results are consistent with the findings of Cheng et al. and Buang et al. [55, 56]. The significant XRD patterns of the pristine MWCNTs observed at 2θ of 25.4° and 42.4° were corresponded to (002) and (100) planes of the carbon atoms, respectively. The same (002) reflection peak was also observed in the case of functionalized MWCNTs, but the intensity of the peak was relatively higher compared to pristine MWCNT. This indicated that after acid treatment the structures were changed in the interlayer spacing of MWCNTs owing to the introduction of functional groups [55]. The XRD patterns of both pristine and f-MWCNTs were quite similar, suggesting that the cylindrical wall structure was protected even after undergoing the acid treatment.

Figure 3:

3.2 Viscosities of dope solutions

As the f-MWCNT is expected to have a high contact surface ratio, the addition of it in the dope solution could increase the viscosity of solution. For all the fabricated membranes, the amount of PVP was fixed at 3% and the f-MWCNT concentration was varied from 0.05 to 0.5%. It was physically observed that the addition of f-MWCNT increased the viscosity of the dope solutions as shown in **Fig. 4**. The presence of inorganic materials in dope solution has also delayed phase separation rate, altering the thermodynamic state of the solution and affecting the conformation and dynamics of the polymer. Hence, the formation of fewer finger-like capillaries and

more sponge-like structures were created in the membranes[57]. The reduction of capillaries as a function of viscosity in membrane structures was confirmed by FESEM. Further discussion of the membrane morphology will be provided in **Section 3.3.2.**

Figure 4:

3.3 Membranes

3.3.1 FTIR

Fig. 5 presents the FTIR spectra of differently formulated membranes. In the spectra, the bands at 1249 and 1134 cm^{-1} were attributed to the stretching vibrations of S=O asymmetric and S=O symmetric respectively, while peaks at 1480 and 1570 cm^{-1} corresponded to bending vibration of PES aromatic rings[58]. The broad peak found at 3450 cm^{-1} could confirm the existence of f-MWCNTs in a membrane that was due to abundant -OH groups attached on the surface of MWCNTs. Besides, the slight increase in the peak intensity of 3100 cm^{-1} is the evidence of the presence of alcohol. The FTIR spectra of Mem-NT membrane did not show any prominent changes compared to Mem-1 to Mem-5 membrane. The stronger intermolecular bonding of the O-H stretching vibrations may give rise to broad and intense bands which are often overlaid with peaks due to Fermi resonance interactions O-H stretching [59]. Thus, the FTIR spectra of membranes confirmed the presence of hydrogen bonding at 3400, 3100 and 1650 cm^{-1}.

Figure 5:

3.3.2 FESEM

Fig. 6 presents the cross-sectional and topology micrographs of the PES and PES/NCs based membranes. Membranes with different NCs exhibited different structures and the characteristic asymmetric morphological structure consisted of a dense layer and finger like-structure as observed in Mem-0 membrane [60, 61]. The addition of NCs in the dope solution improved the sponge-like structures of Mem-0 (bare PES) and Mem-NT membranes into very fine, dense finger-like configuration, especially in the membranes of Mem-1 to Mem-3; Mem-5 membrane, however, showed the disappearance of fine capillaries with irregular wide capillaries and formation of sponge and dense layer in the membrane surface.

All PES/NCs membranes tended to display long channel-like structure which progressively transformed to open ends as clearly visible in Mem-3 and Mem-4 membrane. When the concentration of f-MWCNT was increased to 0.2 g and 0.3g in the Mem-3 and Mem-4, respectively; the spongy structure at the bottom of the membrane tended to deform, creating huge voids and making membranes poor in mechanical strength[62]. A change in the rheological properties of the dope, including a change in the viscosity, might influence the distribution of f-MWCNT/PVP NCs in the membrane matrix. As mentioned in **section 3.2**, the addition of NCs with different amount of f-MWCNT affects the kinetics of phase separation and high viscous dope solution delays the solvent exchange rate with coagulation bath which ultimately result in spongy membrane formation [57]. Both PVP and f-MWCNT play important roles in contributing -COOH and -OH groups to final polymeric membranes produced. The presence of NCs generates instability within the polymer solution and increases the exchange rate between solvent and water in the coagulation bath due to the increased hydrophilic effect compared to the pristine PES membrane. The Mem-5 membrane which showed the highest value of viscosity (**Fig. 4**) due to the high amount of f-MWCNT embedded, did not seem good to develop a regular capillary system in the membrane. Moreover, poor dispersion of NCs especially aggregation of f-MWCNT in Mem-5 was also observed by a 3D picture of AFM **(Fig. 7)**, which might be responsible to its poor dispersion and ultimately affected its morphology.

Figure 6:

3.3.3 Dispersion of NCs and surface roughness

Figure 7 represents the 3D structure of all formulated membranes, whereas **Table 2** shows their quantitative measurements of line statistics with different parameters. In the 3D pictures, white and brown colours demonstrate the presence of different surface heights, whereas in Mem-1 to Mem-5, the white color spine shaped structures represent the aggregation of NCs (especially f-MWCNT). From these 3D images, it is clear that the surface properties of the prepared membranes were altered upon the addition of NCs. In all the NCs based membranes, Mem-5 showed the maximum accumulation of NCs followed by Mem-4.. **Fig. 8** shows the dispersion of f-MWCNTs in the form of NCs in membrane matrix, observed via FESEM. These surface images showed that dispersion quality of NCs was depended on the quantity of f-MWCNT added. As the amount of f-MWCNT was increased from 0.1 to 0.5 g, the dispersion quality decreased in the membrane. The Mem-2 and Mem-3 showed almost similar result, but were better result compared to the Mem-4 and Mem-5. A significant agglomeration of NCs was found in Mem-5. The observation was in good agreement with the 3D AFM image (**Fig. 7**) which also pointed that 0.5 g of f-MWCNT (Mem-5) is not suitable to be used with 3 g of PVP for homogeneous distribution in PES matrix. The ideal loading is therefore between 0.3 and 0.5 as used in Mem-1 to Mem-3. The 3D diagrams of Mem-1 to Mem-3 showed comparatively better distribution of NCs in the membrane matrix, suggesting that the membranes were made of a good relevant ratio (f-MWCNT/PVP with PES). The poor dispersion of NCs also affects the quantitative measurements of line statistics **(Table 2)** and increases the surface roughness parameters with line heights. In the Mem-1 to Mem-4 membranes, the addition of NCs positively decreased the surface roughness (Ra, Rq and Rz) with approximately similar line height profile than Mem-0. The surface roughness of Mem-5 is similar to Mem-0 but its line height profile is quite higher than all other membranes.

Figure 7, 8 and Table 2:

3.3.4 Contact angle and water absorption

Sessile drop contact angle and water absorption experiments are generally used to describe the relative hydrophobicity/hydrophilicity of membranes [63, 64]. Low contact angle and high water absorption values usually mean high hydrophilicity. **Fig. 9** shows the contact angle and water absorption values of pristine PES and PES/NCs membranes. It is observed that the addition of NCs reduced the contact angle from 89.9° to 56.1° and increased water absorption from 27.1 to >235%. The low contact angle results indicate that NCs were successfully incorporated in the membrane matrix. The contact angle for Mem-0 was observed in the range of 93.9° to 85.8° with average 89.9°, whereas for Mem-NT, 86.6° to 78.2° with an average of 83.4° was recorded. If we compared the highest contact angle of Mem-NT with the lowest value of Mem-0, it is found that both membranes displayed similar result. However, the average contact angle of both membranes that was determined based on 15 different measurements was varied by 7.7%. This indicated that the addition of f-MWCNT (in the absence of PVP) in the Mem-NT did play a role in decreasing membrane contact angle. Moreover, its contact angle was much lower compared to the PES/PVP/DMF membrane (average 70.4°), suggesting the role of additives in improving membrane hydrophilicity. **Fig. 9** also shows the progressive decline of contact angle and incline of water absorption results from Mem-0 to Mem-4. The Mem-4 has a smaller contact angle (56.1°) than Mem-5, although the amount of f-MWCNT was higher in Mem-5. This phenomenon suggested that some of the NCs might be eluded from Mem-5 during the phase inversion process.

Figure 9:

3.4 Surface profile and pure water flux

The blending of NCs into PES polymer changed the surface chemistry than pristine PES membrane as observed by grain analysis study of membranes. **Fig. 10** represents the volume, area, perimeter, length, radius and diameter of grains present on the membrane surface. As discussed previously, the addition of NCs to PES improved the grain diameter, length and perimeters of pristine PES membrane **(Fig. 6)**. The pure water flux (J_{w1}) was measured to evaluate the influence of NCs on the membrane permeability (**Fig. 11)**. The J_{w1} values gradually increased with increasing fraction of f-MWCNT into the NCs to 0.3 wt% (Mem-4) and then decreased in the Mem-5. Low contact angle **(Fig. 9)** and reduced capillary system (**Fig. 6**) of Mem-5 clearly explained the reduction of its flux in comparison to Mem-4. The Mem-2 showed the large area and perimeter of grains, but it has a lower value of the flux rate, which can be correlated, to the lower hydrophilicity, water uptake and pore diameter results. The flux rate of pristine PES and Mem-NT membrane was very low, recording 12.94 and 21.19 L/h.m^2 respectively, as shown in **Fig. 11**. Nevertheless, the addition of NCs as additives improved the flux rate, especially as found in Mem-4 (97.54 L/h.m^2). The high hydrophilicity and larger value of grain volume, area and pore diameter coupled with higher surface roughness might be responsible for elevated J_{w1} of Mem-4.

Figure 10 and 11:

3.5 Antifouling properties of membranes

The antifouling performance of the hybrid membranes was evaluated in terms of static and dynamic protein adsorption, flux recovery ratio and membrane resistance parameters. The adsorbed amounts of BSA are presented in **Fig. 12**. The effective reduction in the adsorbed protein amount occurred since BSA was excluded by the tight hydration layer on the membrane surface[15]. In all the membranes, the protein adsorption at dynamic condition was higher than the static one. It might be due to the stirring condition in the dynamic phase that forced the protein molecules to move inside the membrane pores. Whereas, in the case of static adsorption the stirring force was absent and the protein adsorption was mainly occurred on the surface of membranes. These results were similar to the findings reported by Nakamura and Matsumoto in which they compared the protein adsorption rate under the static and dynamic condition [65]. It was observed that in dynamic state multilayer of protein adhesion on the membrane surface was mainly responsible to the high adsorption compared to the static adhesions. In our work, it was found that Mem-2 exhibited the maximum repulsion in comparison to the other membranes in both static and dynamic experiments. The adsorbed amount of BSA (dynamic) on the Mem-5 was found to be 41.9 ug/cm^2, which was 24.4% higher than Mem-2, but still 18.4% lower than pristine membrane (Mem-0). The Mem-NT also showed lower protein adhesion than Mem-0 but higher as compared to PVP/f-MWCNT nanocomposites based membranes. The higher adhesion properties of Mem-NT might be due to its relatively high hydrophobicity, as expressed by its contact angle of 83.4°.

The hydrophobic character of pristine PES membrane is the significant weakness that directly related to membrane fouling as claimed by Khulbe et al. and Van der Bruggen [66, 67]. According to Kelly and Zydne, hydrophobicity increased the protein adhesion on the membrane surface and resulted in more severe fouling [68]. Reihanian et al. reported that the hydrophobic membranes declined in permeability with increasing concentration of protein, whereas highly hydrophilic cellulosic membrane showed no significant BSA adsorption [69]. Membrane with hydrophilic surface in general shows relatively low adsorption of proteins compared to hydrophobic membrane [70]. The incorporation of hydrophilic NCs (f-MWCNT/PVP) has decreased the hydrophobicity of PES membrane which further improved its fouling resistance, as evidenced in Mem-1 and Mem-2. Higher BSA fouling found in the Mem-3 and Mem-4 might be due to the aggregation of NCs which increased surface roughness and negatively affected antifouling property.

Figure 12:

The results for the fouling test are presented in **Fig. 13**. There was a sharp decreased in the flux for all formulated membranes when water was replaced by BSA solution. This result was due to the fouling induced by the adsorption and deposition of the proteins on the membrane surface. A deeper comparison may be obtained from the data presented in **Fig. 14**. Based on this figure, flux recovery

ratio (R_{FR}), total resistance (R_t) and reversible resistance (R_r) was increased while irreversible resistance (R_{ir}) was decreased for all NCs based membranes on comparison to Mem-0 membrane. The main reason might be due to the higher hydrophobicity of the Mem-0, as expressed by the highest contact angle (89.9°) and lower water absorption. The fouling resistance of Mem-NT was slightly better than Mem-0 and comparable with Mem-1, but its flux rate was 45% lower than Mem-1. Mem-2 and Mem-3 showed the best R_{FR} and resistance parameters. Mem-2 displayed the higher R_{FR} (81.7% in the 1st round and 72.2% in the 2nd round of BSA solution) but the R_t, R_r and R_{ir} ratio of Mem-3 was more impressive than other membranes. The higher R_{FR} of Mem-2 might be due to its comparatively lower Ra and protein adsorption than Mem-3. The Mem-3 membrane that displayed relatively lower CA might be responsible for the good R_t, and R_{ir} ratios. The low R_{ir} value indicates the superior ability of membrane surface against protein fouling.

Figure 13 and 14:

3.6 Ultrafiltration of protein

Fig. 15 shows the separation performance of membranes in removing BSA, pepsin, trypsin and lysozyme using a feed solution containing single solute. The rejection rate of solute improved with increasing NCs loading in the PES membrane matrix. The results are consistent with AFM analysis in which decrease the membrane grain diameter resulted in highest rejection rate. In this experiment, Mem-2 membrane achieved the best rejection rate of protein solutes in comparison to the rest of the fabricated membranes, which was also correlated with their grain diameter and radius.

Figure 15:

Conclusion

Low fouling nanocomposite UF membranes were successfully fabricated from blends of f-MWCNT/PVP based NCs with PES polymer by the phase inversion method. The membranes exhibited an asymmetric structure with a relatively fully developed finger-like macrovoids. The FTIR analysis proved that NCs were successfully embedded within PES membrane matrix and played an effective role in improving membrane flux and hydrophilicity. The NC-based membranes had relatively low protein adsorption and irreversible protein fouling than the Mem-0 membrane. The AFM proved to be a good tool to observe the smooth dispersion of NCs and in the Mem-4 and 5 membranes, aggregations of NCs increased the Ra values which in turn enhanced the protein adsorption. The addition of NCs improved the antifouling properties with membrane resistance, especially reversible resistance in Mem-2 and Mem-3 membrane. Results revealed that compared to the pristine PES membrane, the antifouling ability of PES membrane incorporated with f-MWCNT/PVP NC is greater, recording 81.7% flux recovery and 80.2% total resistance (> 76% were reversible one). The protein separation results revealed that, the NCs based membrane was able to reject 93.4%, 74.7%, 59.4% and 28.5% for bovine serum albumin (66 kDa), pepsin (34.6 kDa), trypsin (20 kDa) and lysozyme (14.6 kDa), respectively.

References:

1. J.-C. Janson, *Protein purification: principles, high resolution methods, and applications*, John Wiley & Sons, 2012.
2. T. M. Przybycien, N. S. Pujar and L. M. Steele, *Current opinion in biotechnology*, 2004, **15**, 469-478.
3. A. Saxena, B. P. Tripathi, M. Kumar and V. K. Shahi, *Advances in colloid and interface science*, 2009, **145**, 1-22.
4. M. Kumar and M. Ulbricht, *Polymer*, 2014, **55**, 354-365.
5. C. C. Striemer, T. R. Gaborski, J. L. McGrath and P. M. Fauchet, *Nature*, 2007, **445**, 749-753.
6. C. Casey, T. Gallos, Y. Alekseev, E. Ayturk and S. Pearl, *Journal of Membrane Science*, 2011, **384**, 82-88.
7. M. I. Shukoor, F. Natalio, M. N. Tahir, V. Ksenofontov, H. A. Therese, P. Theato, H. C. Schröder, W. E. Müller and W. Tremel, *Chemical Communications*, 2007, 4677-4679.
8. S. Galier and H. R.-d. Balmann, *Separation and Purification Technology*, 2011, **77**, 237-244.
9. M. Ulbricht, *Polymer*, 2006, **47**, 2217-2262.
10. J.-J. Qin, M. H. Oo and Y. Li, *Journal of membrane science*, 2005, **247**, 137-142.
11. H. Yamamura, K. Kimura and Y. Watanabe, *Environmental science & technology*, 2007, **41**, 6789-6794.
12. Y.-F. Zhao, L.-P. Zhu, Z. Yi, B.-K. Zhu and Y.-Y. Xu, *Journal of Membrane Science*, 2013, **440**, 40-47.
13. D. Y. Koseoglu-Imer, B. Kose, M. Altinbas and I. Koyuncu, *Journal of Membrane Science*, 2013, **428**, 620-628.
14. L.-Y. Yu, Z.-L. Xu, H.-M. Shen and H. Yang, *Journal of Membrane Science*, 2009, **337**, 257-265.
15. E. Celik, L. Liu and H. Choi, *water research*, 2011, **45**, 5287-5294.
16. S. Maphutha, K. Moothi, M. Meyyappan and S. E. Iyuke, *Scientific reports*, 2013, **3**.
17. J. María Arsuaga, A. Sotto, G. del Rosario, A. Martínez, S. Molina, S. B. Teli and J. de Abajo, *Journal of Membrane Science*, 2013, **428**, 131-141.
18. A. Razmjou, J. Mansouri and V. Chen, *Journal of Membrane Science*, 2011, **378**, 73-84.

19. W. Lu and T.-W. Chou, *Journal of the Mechanics and Physics of Solids*, 2011, **59**, 511-524.
20. P.-C. Ma, N. A. Siddiqui, G. Marom and J.-K. Kim, *Composites Part A: Applied Science and Manufacturing*, 2010, **41**, 1345-1367.
21. X.-L. Xie, Y.-W. Mai and X.-P. Zhou, *Materials Science and Engineering: R: Reports*, 2005, **49**, 89-112.
22. C. A. Dyke and J. M. Tour, *The Journal of Physical Chemistry A*, 2004, **108**, 11151-11159.
23. D. Qian, E. C. Dickey, R. Andrews and T. Rantell, *Applied physics letters*, 2000, **76**, 2868-2870.
24. E. Choi, J. Brooks, D. Eaton, M. Al-Haik, M. Hussaini, H. Garmestani, D. Li and K. Dahmen, *Journal of Applied physics*, 2003, **94**, 6034-6039.
25. J.-P. Salvetat, G. A. D. Briggs, J.-M. Bonard, R. R. Bacsa, A. J. Kulik, T. Stöckli, N. A. Burnham and L. Forró, *Physical review letters*, 1999, **82**, 944.
26. L. Jin, C. Bower and O. Zhou, *Applied physics letters*, 1998, **73**, 1197-1199.
27. J. Sun and L. Gao, *Carbon*, 2003, **41**, 1063-1068.
28. K. Mukhopadhyay, C. D. Dwivedi and G. N. Mathur, *Carbon*, 2002, **40**, 1373-1376.
29. C. Schmid and D. Klingenberg, *Physical Review Letters*, 2000, **84**, 290.
30. H. Touhara, A. Yonemoto, K. Yamamoto, S. Komiyama, S. Kawasaki, F. Okino, T. Yanagisawa and M. Endo, 2004.
31. B. McCarthy, J. Coleman, R. Czerw, A. Dalton, D. Carroll and W. Blau, *Synthetic Metals*, 2001, **121**, 1225-1226.
32. J. Liu, A. G. Rinzler, H. Dai, J. H. Hafner, R. K. Bradley, P. J. Boul, A. Lu, T. Iverson, K. Shelimov and C. B. Huffman, *Science*, 1998, **280**, 1253-1256.
33. Q. Yang, T.-S. Chung and M. Weber, *Journal of Membrane Science*, 2009, **326**, 322-331.
34. M. Sun, Y. Su, C. Mu and Z. Jiang, *Industrial & Engineering Chemistry Research*, 2009, **49**, 790-796.
35. J. Barzin, S. Madaeni, H. Mirzadeh and M. Mehrabzadeh, *Journal of applied polymer science*, 2004, **92**, 3804-3813.
36. N. Poorgholami-Bejarpasi and B. Sohrabi, *Fluid Phase Equilibria*, 2015, **394**, 19-28.
37. S. Niyogi, M. Hamon, H. Hu, B. Zhao, P. Bhowmik, R. Sen, M. Itkis and R. Haddon, *Accounts of Chemical Research*, 2002, **35**, 1105-1113.
38. N. R. Raravikar, L. S. Schadler, A. Vijayaraghavan, Y. Zhao, B. Wei and P. M. Ajayan, *Chemistry of materials*, 2005, **17**, 974-983.
39. X. Chang, Z. Wang, S. Quan, Y. Xu, Z. Jiang and L. Shao, *Applied Surface Science*, 2014, **316**, 537-548.
40. Z.-X. Wang, C.-H. Lau, N.-Q. Zhang, Y.-P. Bai and L. Shao, *Journal of Materials Chemistry A*, 2015, **3**, 2650-2657.
41. G.-X. Chen, H.-S. Kim, B. H. Park and J.-S. Yoon, *The Journal of Physical Chemistry B*, 2005, **109**, 22237-22243.
42. C. M. Kee and A. Idris, *Separation and Purification Technology*, 2010, **75**, 102-113.
43. R. Guan, H. Zou, D. Lu, C. Gong and Y. Liu, *European Polymer Journal*, 2005, **41**, 1554-1560.
44. Z.-K. Xu, F.-Q. Nie, C. Qu, L.-S. Wan, J. Wu and K. Yao, *Biomaterials*, 2005, **26**, 589-598.
45. Microsoft Word - XEI 1.5 Manual _Release Candidate_.doc - XEImagingSoftwareManual.pdf, http://research.fit.edu/nhc/documents/XEImagingSoftwareManual.pdf).
46. L. Shao, Z. X. Wang, Y. L. Zhang, Z. X. Jiang and Y. Y. Liu, *Journal of Membrane Science*, 2014, **461**, 10-21.
47. G. Arthanareeswaran, T. S. Devi and M. Raajenthiren, *Separation and Purification Technology*, 2008, **64**, 38-47.
48. Q. Yang, Z.-K. Xu, Z.-W. Dai, J.-L. Wang and M. Ulbricht, *Chemistry of materials*, 2005, **17**, 3050-3058.
49. H. T. Ham, Y. S. Choi and I. J. Chung, *Journal of Colloid and Interface Science*, 2005, **286**, 216-223.
50. K. Balasubramanian and M. Burghard, *Small*, 2005, **1**, 180-192.
51. M. Irfan, A. Idris, N. M. Yusof, N. F. m. khairuddin and H. Akhmal, *Journal of membrane science*, 2014.
52. R. Sepahvand, M. Adeli, B. Astinchap and R. Kabiri, *Journal of Nanoparticle Research*, 2008, **10**, 1309-1318.
53. W. Caminati, A. Dell'Erba, G. Maccaferri and P. G. Favero, *Journal of molecular spectroscopy*, 1998, **191**, 45-48.
54. M. Irfan, A. Idris, N. M. Yusof, N. F. M. Khairuddin and H. Akhmal, *Journal of Membrane Science*, 2014, **467**, 73-84.

55. Y. Cheng, W. Li, X. Fan, J. Liu, W. Xu and C. Yan, *Electrochimica Acta*, 2013, **111**, 635-641.
56. N. A. Buang, F. Fadil, Z. A. Majid and S. Shahir, *Digest Journal of Nanomaterials and Biostructures*, 2012, **7**, 33-39.
57. B. Torrestiana-Sanchez, R. Ortiz-Basurto and E. Brito-De La Fuente, *Journal of membrane science*, 1999, **152**, 19-28.
58. J.-H. Choi, J. Jegal and W.-N. Kim, *Journal of Membrane Science*, 2006, **284**, 406-415.
59. N. Giri, R. Natarajan, S. Gunasekaran and S. Shreemathi, *Archives of Applied Science Research*, 2011, **3**, 624-630.
60. M. Taniguchi, J. E. Kilduff and G. Belfort, *Journal of Membrane Science*, 2003, **222**, 59-70.
61. M. Taniguchi and G. Belfort, *Journal of membrane science*, 2004, **231**, 147-157.
62. C. Barth, M. Goncalves, A. Pires, J. Roeder and B. Wolf, *Journal of Membrane Science*, 2000, **169**, 287-299.
63. A. Idris, N. Mat Zain and M. Noordin, *Desalination*, 2007, **207**, 324-339.
64. A. Idris, K. Y. Hew and M. K. Chan, *Jurnal Teknologi (Kejuruteraan)*, 2009, 67-76.
65. K. Nakamura and K. Matsumoto, *Journal of membrane science*, 2006, **285**, 126-136.
66. K. Khulbe, C. Feng and T. Matsuura, *Journal of applied polymer science*, 2010, **115**, 855-895.
67. B. Van der Bruggen, *Journal of applied polymer science*, 2009, **114**, 630-642.
68. S. T. Kelly and A. L. Zydney, *Biotechnology and bioengineering*, 1997, **55**, 91-100.
69. H. Reihanian, C. Robertson and A. Michaels, *Journal of Membrane Science*, 1983, **16**, 237-258.
70. J. Y. Park, M. H. Acar, A. Akthakul, W. Kuhlman and A. M. Mayes, *Biomaterials*, 2006, **27**, 856-865.

Tables and Figures:

Table 1: Formulation of PES and nanocomposite based membranes.

Formulation (wt. %)				
Membrane designation	Nanocomposites			PES
	f-MWCNT	PVP	DMF	
Mem-0	--	--	84	16
Mem-NT	0.2	--	83.8	16
Mem-1	0.05	3	80.95	16
Mem-2	0.1	3	80.9	16
Mem-3	0.2	3	80.8	16
Mem-4	0.3	3	80.7	16
Mem-5	0.5	3	80.5	16

Table 2: The quantitative measurements of line statistics table, represent the reading of two selected lines in the X and Y axis cross sections via XEI standard software of scanned AFM images.

Mem-#	Line axis	Min (nm)	Max (nm)	Mid (nm)	Rpv (nm)	Rq (nm)	Ra (nm)	Rz (nm)	Rsk	Rku
Mem-0	X	-27	28.5	0.84	55.4	12.3	10.1	48.5	0.06	2.36
	Y	-21	32.4	5.48	53.7	10.9	8.74	43.6	-0.4	2.65
Mem-1	X	-13	18.3	2.55	31.5	5.68	4.54	22.4	-0.5	3.05
	Y	-18	12.8	-2.5	30.6	6.68	5.51	26	0.12	2.29
Mem-2	X	-13	12	-0.5	25	5.7	4.77	20.6	0.17	2.2
	Y	-12	8.2	-1.9	20.2	4.08	3.27	15.4	0.56	2.78
Mem-3	X	-17	20.8	1.9	37.9	8.51	7.15	33.7	-0.3	2.27
	Y	-15	19.8	2.54	34.5	8.76	7.56	30.7	-0.4	2.05
Mem-4	X	-18	27.7	4.95	45.5	8.89	6.73	32.6	-0.5	3.41
	Y	-9.5	33	11.7	42.5	6.34	3.77	23.5	-2.8	12.4
Mem-5	X	-15	70.6	28	85.1	12.9	7.88	33.1	-3.6	17.7
	Y	-6.2	73.1	33.5	79.3	11.9	5.83	30.9	-4	20.4

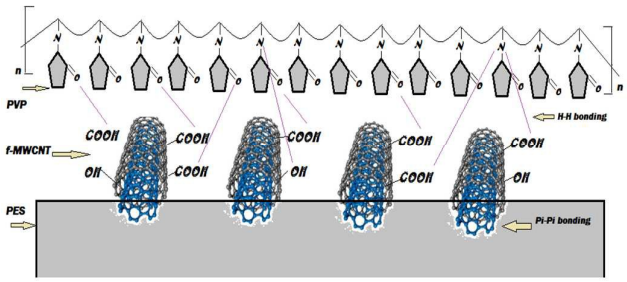

Figure 1: Schematic representation of NCs (f-MWCNT/PVP) based PES membranes.

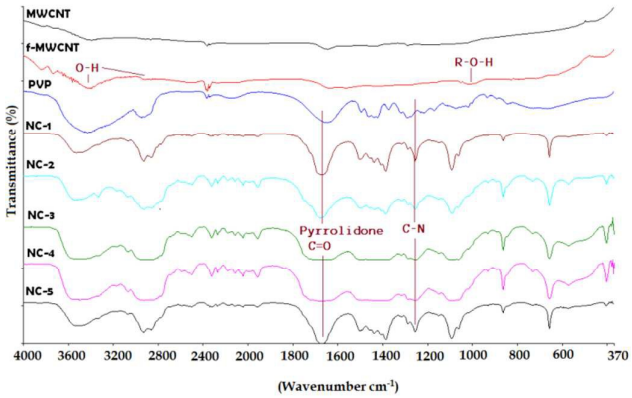

Figure 2: FTIR spectra of MWCNT, f-MWCNT and NCS (PVP/f-MWCNT in DMF).

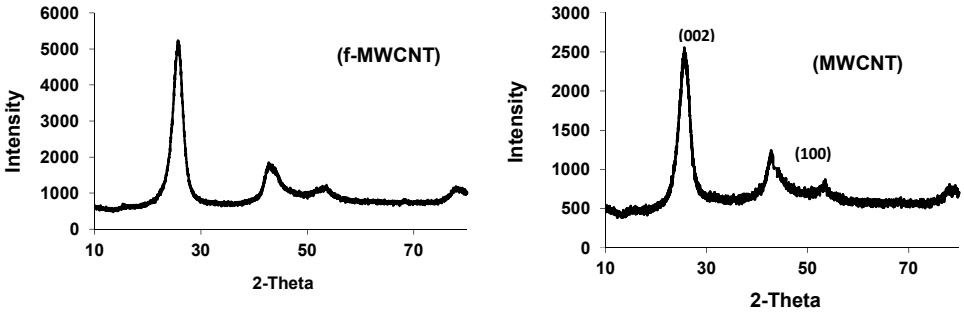

Figure 3: XRD results of MWCNT and f-MWCNT.

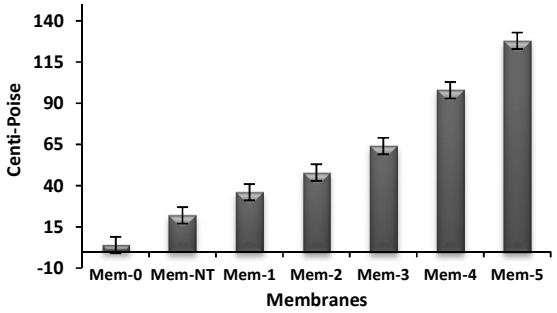

Figure 4: Viscosities of dope solutions used for membrane making.

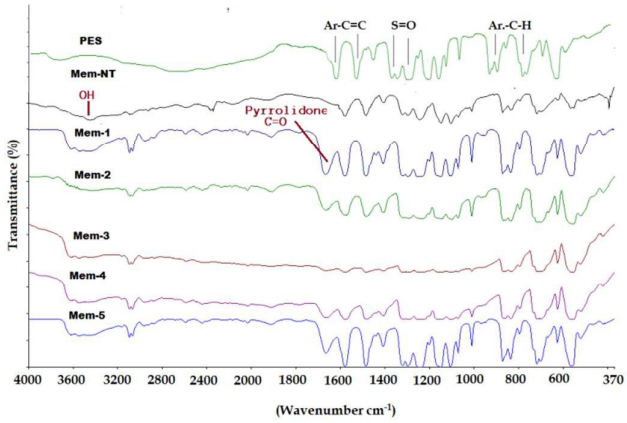

Figure 5: FTIR spectra of all the fabricated membranes.

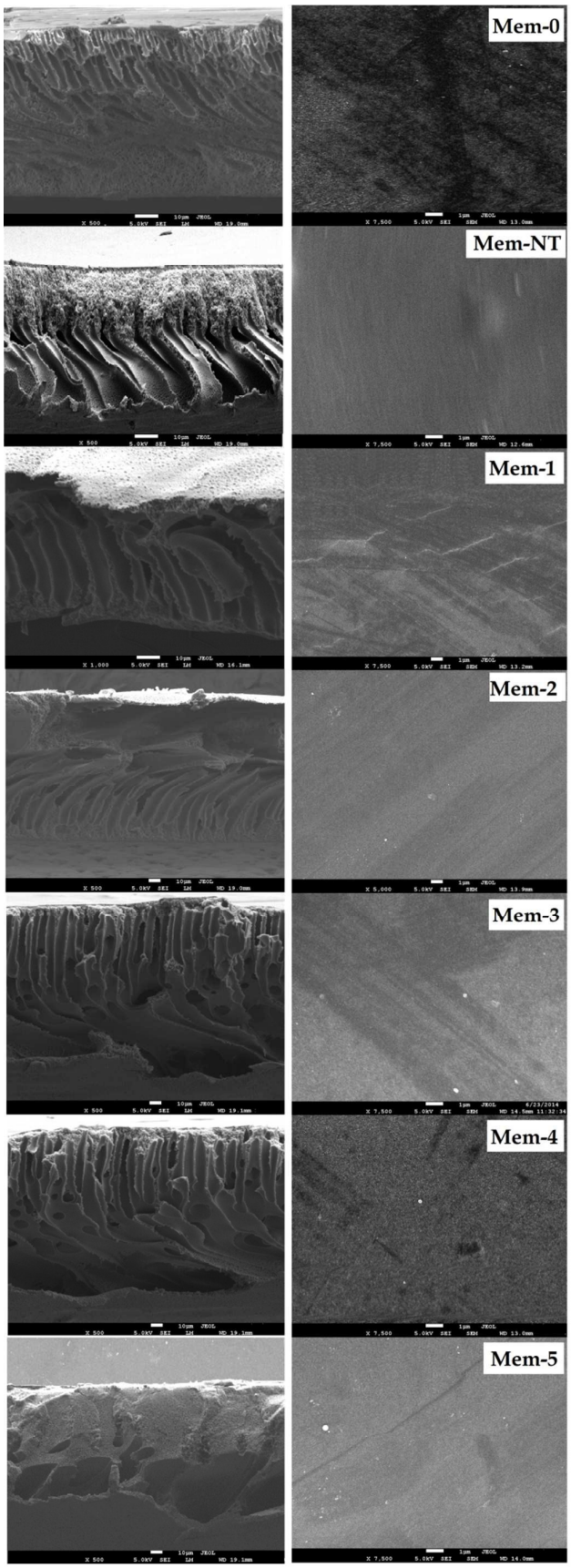

Figure 6: FESEM cross section and surface topology images of PES and NCs membranes.

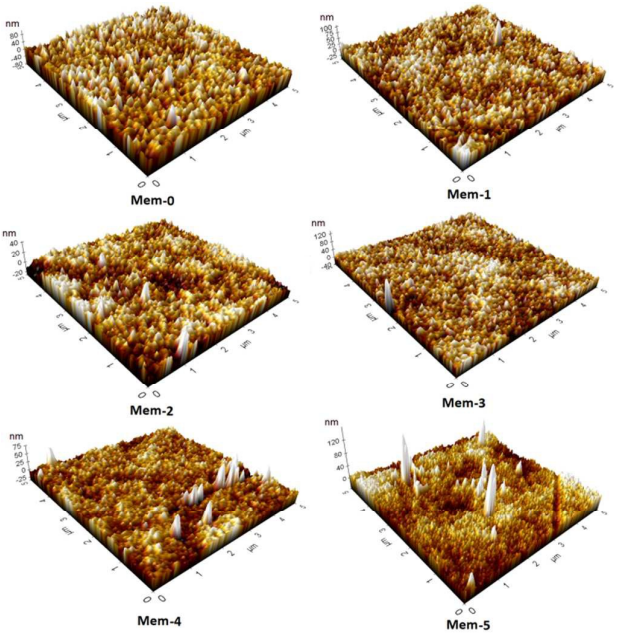

Figure 7: The AFM 3D pictures of surface roughness of all formulated membranes. The white erected line shows the aggregation of NCs.

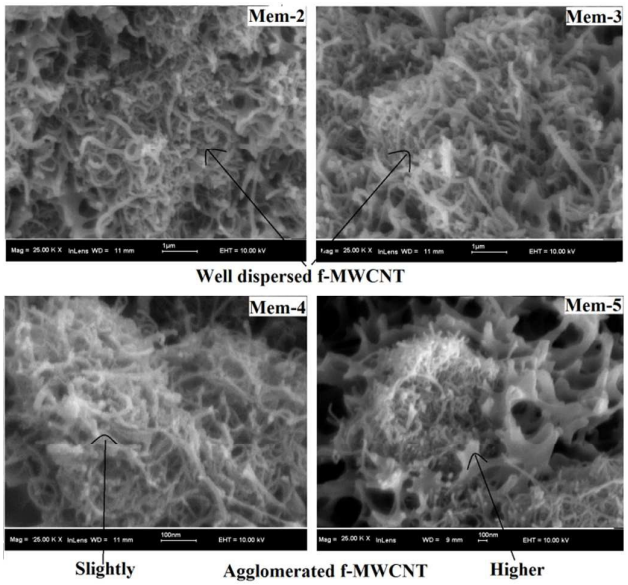

Figure 8: Dispersion behavior of NCs into the membrane at 25K magnification.

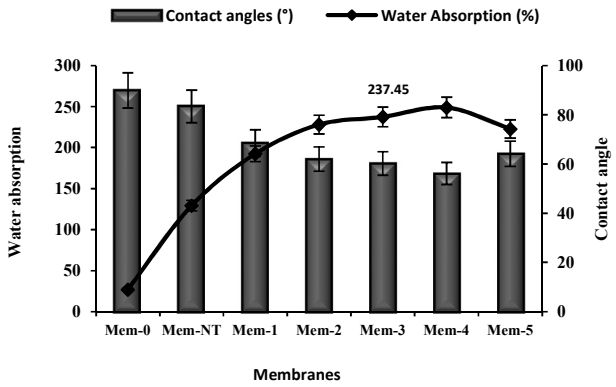

Figure 9: The contact angle and water absorption of PES and PES/NCs based membranes.

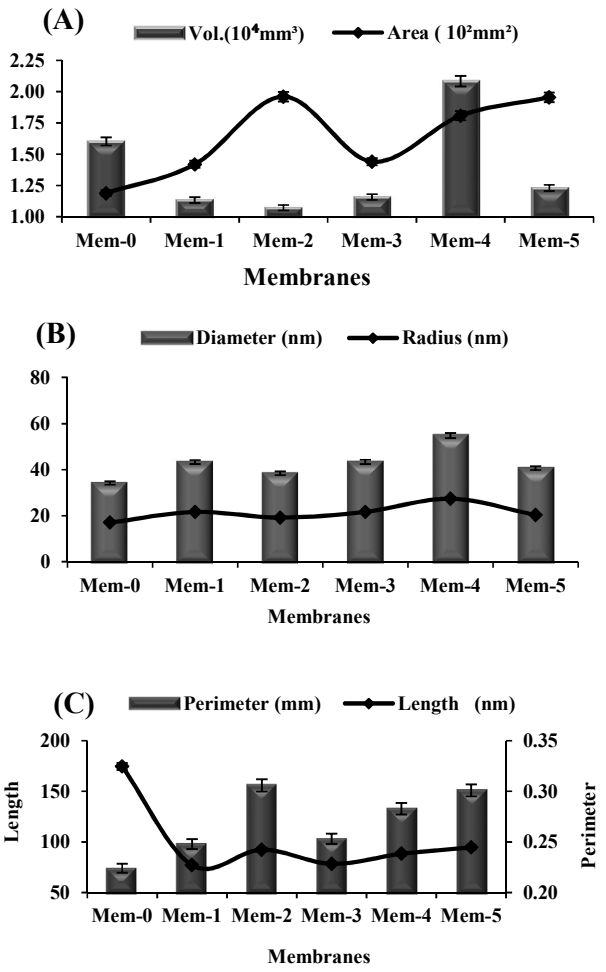

Figure 10: Surface profiles of all formulated membranes, obtained via XEI-AFM software of scanned images. A) - Volume and area of grains, B) radius and diameter of surface grain and, C) – perimeter and length of grains.

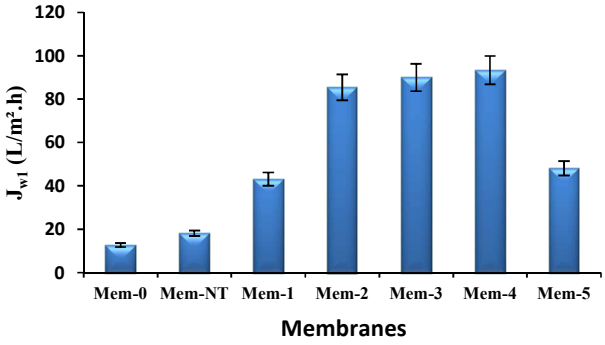

Figure 11: Pure water flux of all fabricated membranes.

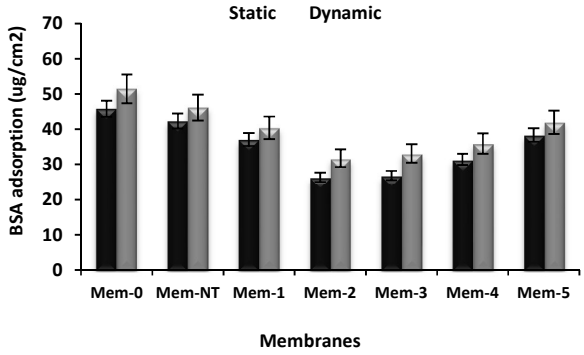

Figure 12: Protein adsorption of all fabricated membranes.

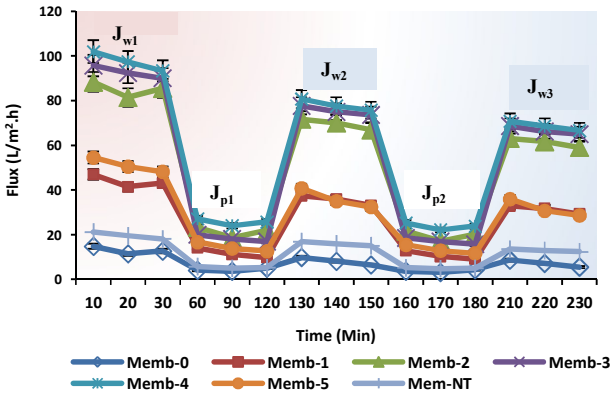

Figure 13: Time-dependent flux of all fabricated membranes before and after modification under two cycles of BSA solution ultrafiltration tests

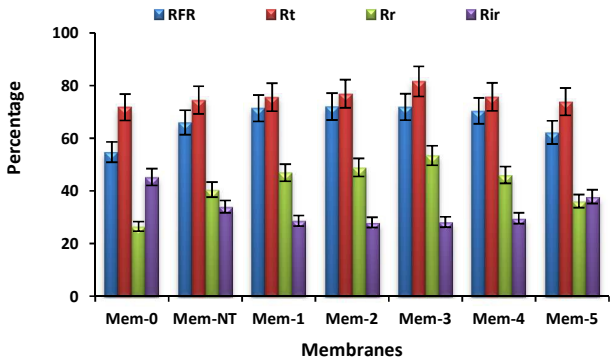

Figure 14: Fouling parameters for all fabricated membranes with respect to R_{FR}, R_t, R_r and R_{ir}.

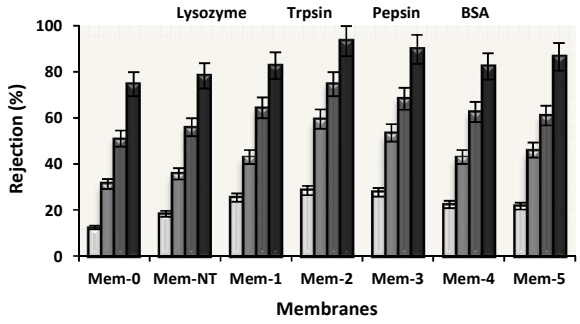

Figure 15: Separation performance of membranes in removing BSA, pepsin, trypsin and lysozyme using feed solution containing 1000 ppm solute.